Energy & Environmental Science

COMMUNICATION

View Article Online
View Journal | View Issue

Cite this: *Energy Environ. Sci.*, 2017, **10**, 2516

Received 21st September 2017,
Accepted 13th November 2017

DOI: 10.1039/c7ee02716h

rsc.li/ees

Electro-synthesis of ammonia from nitrogen at ambient temperature and pressure in ionic liquids†

Fengling Zhou, Luis Miguel Azofra, Muataz Ali, Mega Kar, Alexandr N. Simonov, Ciaran McDonnell-Worth, Chenghua Sun, Xinyi Zhang and Douglas R. MacFarlane *

Ammonia as the source of most fertilizers has become one of the most important chemicals globally. It also is being increasingly considered as an easily transported carrier of hydrogen energy that can be generated from "stranded" renewable-energy resources. However, the traditional Haber–Bosch process for the production of ammonia from atmospheric nitrogen and fossil fuels is a high temperature and pressure process that is energy intensive, currently producing more than 1.6% of global CO_2 emissions. An ambient temperature, electrochemical synthesis of ammonia is an attractive alternative approach, but has, to date, not been achieved at high efficiency. We report in this work the use of ionic liquids that have high N_2 solubility as electrolytes to achieve high conversion efficiency of 60% for N_2 electro-reduction to ammonia on a nanostructured iron catalyst under ambient conditions.

Broader context

Ammonia is being widely considered as a sustainable fuel that could be produced from renewable energy. This could provide a sink for excess energy in the grid at times of excess supply, or alternatively could be installed in remote areas where the scope for generation of solar or wind energy is immense. The transportation technology for ammonia is already well established, either by bulk tanker or by pipeline. At point of use it can be cracked into hydrogen, or used directly in engines or gas turbines. The roadblock to large scale use of ammonia as a fuel is the need for a high efficiency means of its production from atmospheric nitrogen, water and renewable energy. Here we describe the direct electrochemical reduction of nitrogen to ammonia at high efficiency under ambient conditions. High efficiency is achieved by virtue of a family of ionic liquid electrolytes (salts that are liquid at ambient temperatures) that offer unusually high solubility for N_2. They also possess a hydrophobic nature that allows the water content to be controlled at an optimum level that supports ammonia production, but minimises the competing production of hydrogen. The process thus paves the way to the "Ammonia Economy".

There is enormous capacity for renewable energy generation in remote, high insolation areas of the world, however the delivery of the energy in a transportable form to population centres is a challenging issue. Ammonia (NH_3) is one of the most widely produced chemicals worldwide; while most production is currently for use as fertilizers, it is also being considered as an easily transportable "energy store" for renewable energy. Ammonia is industrially synthesized *via* the Haber–Bosch process from N_2 and H_2 at high temperature and pressure through the reaction:

$$N_2 + 3H_2 \Leftrightarrow 2NH_3$$

The harsh conditions involved render this reaction less energy efficient than is desirable for either sustainable fertilizer production, or for use as an energy carrier. Thus, there is growing interest in alternative and sustainable approaches to ammonia synthesis, in particular by electrochemical reduction.[1–21] Several groups have investigated the reduction of N_2 to NH_3 from aqueous or alcohol-based solutions at room temperature at a variety of electrodes.[22–26] However, only impractically low current-conversion efficiency (also known as faradaic efficiency, FE), below 7%, has been achieved.[22,27] Licht *et al.* have recently reported an ammonia electro-synthesis from N_2 and steam in a molten hydroxide electrolyte containing a nanoscale Fe_2O_3 suspension at 200–250 °C supporting FE as high as 35%.[28] Photo-electrochemical N_2 reduction has also been studied by several groups including us,[4,29–32] however the efficiency of these processes remains low.

A variety of electro-catalysts for N_2 reduction have been investigated both experimentally and theoretically.[2,10,33–39] Quantum chemical calculations for a range of different metal surfaces indicate that Fe, Mo, Rh, and Ru are predicted to be the most catalytically active for N_2 electro-reduction.[34] Among them, Fe is particularly interesting, as it is an inexpensive, earth-abundant element, that is also a key element in N_2 fixation in nitrogenase enzymes, as well as being the most common catalyst in the Haber–Bosch process.[40] Nonetheless, optimisation of the structure and morphology of the electro-catalyst is necessary for high efficiency operation in this N_2 reduction context.

ARC Centre of Excellence for Electromaterials Science and School of Chemistry, Monash University, Clayton, Victoria 3800, Australia.
E-mail: douglas.macfarlane@monash.edu

† Electronic supplementary information (ESI) available: Materials and methods, Fig. S1–S7. See DOI: 10.1039/c7ee02716h

The reason for the low faradaic efficiency of ammonia electro-synthesis is typically the reduction of water to hydrogen that occurs in the same region of potential. This is often dominant, in part because N_2 is only sparingly soluble in most electrolytes. On the other hand, ionic liquids (ILs) can serve as excellent non-aqueous electrolytes[41–44] and, as the water content in ILs can be much lower than in aqueous solutions, H_2 evolution can be effectively suppressed. In addition, certain ILs are known to support high nitrogen solubility at room temperature, as much as 20 times higher than in water on a volumetric basis,[45] making these particular ILs attractive as media for the nitrogen reduction process.

In this work, we demonstrate an electrochemical synthesis of ammonia with faradaic efficiency as high as 60% at ambient temperature and pressure. This high efficiency is achieved *via* the combination of a hydrophobic, high nitrogen-solubility IL electrolyte and a nanostructured Fe-based electrocatalyst. The role and the nature of the ILs, as well as the electrode substrate, are explored to provide a basis for further understanding of this process.

The ILs employed were chosen from those known to exhibit high N_2 solubility: [C_4mpyr][eFAP] and [$P_{6,6,6,14}$][eFAP].[45] The latter, a phosphonium-based IL, was included to eliminate the IL as a possible nitrogen source; its structure and mode of interaction with N_2 (as discussed further below) are shown in Fig. 1a. Full details of materials and methods are provided in the ESI.† Several working electrode substrates were investigated, including fluorine doped tin oxide glass (FTO), nickel foam (NF) and stainless steel cloth (SS). An iron-based catalyst was chosen as one of the known, high-performing N_2 reduction catalysts in the Haber–Bosch process. To optimize the electrochemical activity of the catalyst, it was applied to the electrode substrate by an electro-deposition technique. Nitrogen reduction was conducted in standard electrochemical cells with a flowing gas stream (Fig. S1, ESI†). The synthesized ammonia was transferred from the reaction vessel by the gas stream to a trap containing a weak aqueous acid solution (1 mM H_2SO_4) which was later analyzed. The N_2 gas stream was also analysed to determine the inevitable trace amounts of NH_3 and NO_x. Further details are provided in the ESI.†

Electrochemical nitrogen reduction is illustrated in Fig. 1a for the SS substrate. The scanning electron micrograph (SEM) image of the electrodeposited iron surface on the stainless steel (Fe-SS) substrate is shown in Fig. 1b. The iron layer is composed of ~100 nm aggregates of nanoparticles. The composition and structure of the iron layer was further examined *via* its electron diffraction pattern and high-resolution transmission electron micrograph (HRTEM) as well as X-ray diffraction, Fig. 1c and Fig. S3 (ESI†). These confirm the body-centred cubic structure of the Fe nanocrystals. From electrochemical analysis the roughness factor (RF) of the Fe-SS electrodes was estimated to be about 9 (Fig. S4, ESI†).

Fig. 2a and b show the total current density and the FE for ammonia production for a range of electrode-IL combinations (at 100 ppm H_2O in the IL) as a function of time and potential. The currents rapidly reach stable values (Fig. 2a), the initial transients being double layer charging and the reduction of FeO formed on the surface during cell assembly. To ensure an unambiguous quantification of the N_2 reduction efficiency, we include an IL known to offer a high N_2 solubility ([$P_{6,6,6,14}$][eFAP]),[45] but which does not contain any N-atoms; this ensures that the only source of N in these experiments is the N_2 introduced from the gas phase.

The FE for N_2 reduction to NH_3 as a function of potential is shown in Fig. 2b and as a function of temperature in Fig. S5 (ESI†). The FE passes through a maximum of 60 ± 6% at around −0.8 V *vs.* NHE and then decreases as the potential becomes

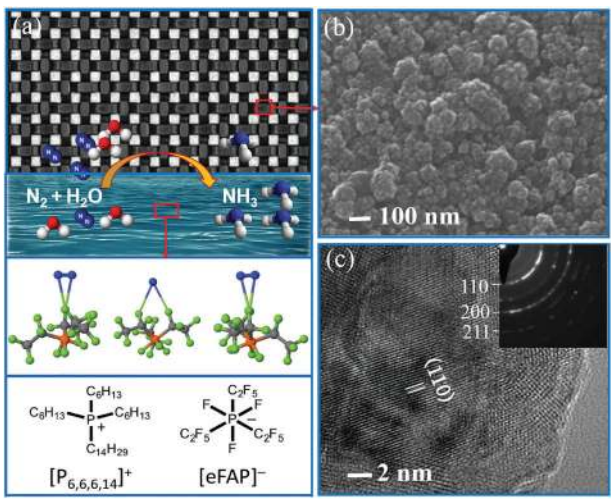

Fig. 1 (a) Schematic of the N_2 reduction process on a Fe-SS electrode. Lower panels: structures of the ionic liquid ions and their interaction with N_2. (b) SEM image of the electrodeposited Fe-catalyst and (c) HRTEM image of Fe particles (inset shows the corresponding electron diffraction pattern).

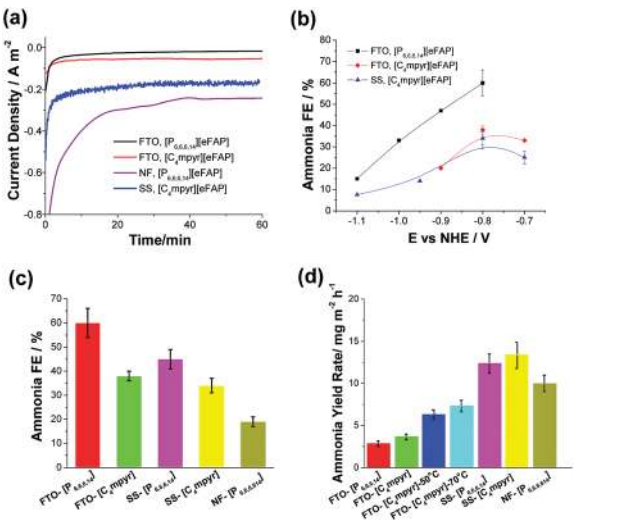

Fig. 2 (a and c) Current density *vs.* time and faradaic efficiency for electro-reduction of N_2-saturated ionic liquids on various electrodes at a constant potential of −0.8 V *vs.* NHE; (b) dependence of faradaic efficiency for ammonia production on potential for various electrode/IL combinations; (d) the ammonia production rate on different electrodes and ionic liquids at −0.8 V *vs.* NHE. In (b–d) the results for FTO and SS substrates are based on a 3 h experiment.

more negative (reductive). On increasing the operating temperature, the FE also exhibits a decreasing trend at higher temperatures, as expected due to the decreasing N_2 solubility. Separate trials confirmed that the only by-product is H_2.

It is important to recognise the ubiquitous presence of small amounts of ammonia and NO_x in the atmosphere, on laboratory surfaces and in gas supplies. Indeed, in the field of photochemical synthesis of ammonia it has been shown that many reported claims were in fact detecting only exogenous contaminants.[46] Thus, in our work various control experiments with no potential applied and/or in the absence of N_2 were undertaken to confirm that there was no significant other source of ammonia or ammonium compounds present as contaminants. Ionic liquid samples for electrochemical trials were washed with aqueous 1 mM KOH until no NH_3 was detectable (LOD 1 nmol ml^{-1}). In blank experiments carried out under conditions identical to those in Fig. 2, but with no voltage applied, no ammonia was detectable. This indicates that there are no laboratory or equipment sources of extraneous ammonia. Further blank experiments were conducted under identical conditions (including applied voltage) to those of Fig. 2, except that the gas stream was high purity Ar. The result was 4.0 ± 0.5 nmol which is indistinguishable from that measured in the absence of potential and also that expected on the basis of the NH_3 content of the Ar gas; note that the 4.0 nmol is significantly smaller than any of the reported results here which typically lie in the 10–50 nmol range. These Ar control experiments indicate that there is no source of ammonia generated in our standard experiments in the absence of N_2. In order to confirm that the ionic liquid is stable in the working potential range we determined that only H_2 is produced on a Pt electrode, with close to 100% faradaic efficiency, at *ca.* −1.1 V in an Ar saturated IL. The excellent performance of the phosphonium ionic liquid for ammonia production in Fig. 2 also serves to further confirm that the IL is not the source of any ammonia, as that compound contains no nitrogen. As a further proof that the detected ammonia results from reduction of N_2, a $^{15}N_2$ reduction experiment was carried out, as described in the ESI,† demonstrating the production of $^{15}NH_3$. In summary, these vital control experiments demonstrate that the ammonia detected is electrochemically produced by reduction of N_2.

Fig. S6 (ESI†) shows that the cyclic voltammetric response depends strongly on the water content. The FE remained approximately constant at 38 ± 4% when the concentration of H_2O was varied from 20 to 250 ppm. Water is the sole proton source in the process, therefore maintenance of some level of water is necessary. However, it appears that the catalyst selectivity is not strongly influenced by the water content within the examined range.

While the Fe-FTO electrode provides high FE, the reduction currents obtained on this low surface area substrate are too small for practical application. Design of FTO-type coatings on high surface area substrates holds promise for improving the applicability of this type of electrode. A variety of high surface area substrates were employed here to increase the working surface area. Fig. 2 shows that the current density (per unit geometric surface area) increases on using these porous substrates. For example, the current density increases in $[P_{6,6,6,14}][eFAP]$ from 0.012 A m^{-2} for FTO to 0.1 A m^{-2} for SS and 0.3 A m^{-2} for NF, with corresponding faradaic efficiencies (Fig. 2c) of 60%, 45% and 19% respectively. This enhancement produces significant increases in the production rates of NH_3 (Fig. 2d), for example from 2.9 mg m^{-2} h^{-1} on FTO to 14 mg m^{-2} h^{-1} on the SS substrate in $[C_4mpyr][eFAP]$. The decreased faradaic efficiencies on the more porous substrates suggests that N_2 depletion, or build up of NH_3, near the electrode during the reaction is limiting the rate of nitrogen reduction and shifting the balance in favour of proton reduction. Such mass transport limitations are common in electrochemical processes and can be suppressed in advanced cell design. The ammonia yield increases continuously with time (Fig. S7, ESI†), after initially elevated rates while a steady state is established. It is important to note that the SS cathodes used here are quite thin and flexible so that there is considerable scope to further increase yields by optimizing cathode thickness and also to implement high surface area, thin-layer or spiral wound type electrode configurations.

Compared with $[P_{6,6,6,14}][eFAP]$, the $[C_4mpyr][eFAP]$ IL produces higher current densities and yields (Fig. 2) due to its lower viscosity (Fig. S8, ESI†), which supports higher mass transport. The FE in $[C_4mpyr][eFAP]$ is slightly lower than $[P_{6,6,6,14}][eFAP]$, consistent with the differences in N_2 solubility (0.20 mg g^{-1} *vs.* 0.28 mg g^{-1} respectively[45]). Nonetheless, the yield is higher in $[C_4mpyr][eFAP]$, as shown in Fig. 2d. In comparison to recent reports the maximum yield in Fig. 2d at 14 mg m^{-2} h^{-1} at 30% FE compares favourably with the literature, the highest of which at room temperature and pressure is 16 mg m^{-2} h^{-1} at 4% FE.[27] For comparison we have also examined another ionic liquid, $[HMIM][NTf_2]$, which has a much smaller N_2 solubility (<0.017 mg g^{-1}).[47] The faradic efficiency for N_2 reduction in this ionic liquid was found to be much smaller (0.64%).

The reason for the high solubility of N_2 in the selected ILs was further examined by DFT calculations. The interaction of various common anions with N_2 is shown in Fig. 3a and b, where the calculations indicate that the molecule interacts relatively weakly with ions such as Cl^- and with other fluorinated anions

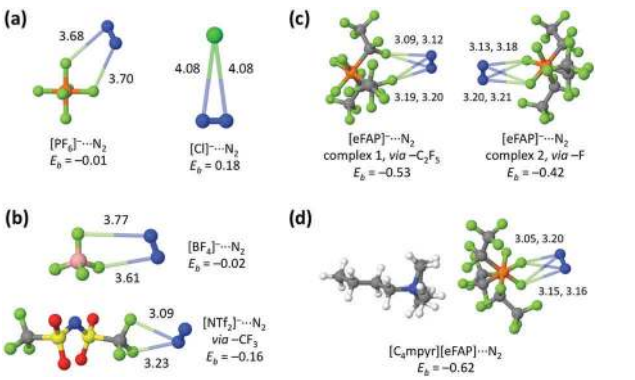

Fig. 3 (a–c) N_2 binding energies (in kcal mol^{-1}) and bond distances in Å for various anions. The interaction with $[eFAP]^-$ in panel (c) shows two distinct modes: complex 1 exhibits C–F interactions and complex 2, P–F interactions. Panel (d) introduces the cation to show the interaction with an ion pair of $[C_4mpyr][eFAP]$; the interaction is the strongest of all those studied.

such as BF_4^- and PF_6^-. On the other hand, the interaction with $[eFAP]^-$ is distinctly stronger, Fig. 3c, where two modes are distinguished: complex 1 reveals the N_2 interacting with the F atoms on the alkyl chains, while complex 2 has the N_2 interacting with the F atoms bound to the phosphorous. It appears that the more strongly delocalized is the negative charge, the stronger is the N_2 binding. The distinction between the binding energy in this $[eFAP]^-$ complex and that with PF_6^- is striking. In the $[eFAP]^-$ case the additional delocalization of charge onto the three C_2F_5 groups modulates the charge on the P-bound fluorine atoms and thereby enhances the interaction with N_2. Introducing the cation into these calculations, Fig. 3d, shows that the interaction becomes even stronger, because of further charge interaction between the anion and the cation.

In summary, we show in this work that the use of high N_2-solubility ionic liquids enables the electro-reduction of N_2 to ammonia at room temperature and atmospheric pressure. This property of these ionic liquids strongly depends on their particular ionic structure. Faradaic efficiencies as high as 60% have been achieved in $[P_{6,6,6,14}][eFAP]$. The yields are currently un-optimized, and there is considerable scope for further development of the catalysts, along with optimization of other parameters such as electrode composition, structure and geometry. We hope that this work will stimulate further interest in this environmentally important area of research.

Conflicts of interest

There are no conflicts to declare.

Acknowledgements

The authors are grateful to the Australian Research Council for funding through the Australian Centre for Electromaterials Science and Grant No. 170102267 and also for DRM's Australian Laureate Fellowship. The authors also acknowledge the use of facilities within the Monash Centre for Electron Microscopy.

References

1 U. S. Depart of Energy, *Sustainable Ammonia Synthesis – Exploring the scientific challenges associated with discovering alternative, sustainable processes for ammonia production*, 2016.
2 C. J. M. v. d. Ham, M. T. M. Koper and D. G. H. Hetterscheid, *Chem. Soc. Rev.*, 2014, **43**, 5183–5191.
3 A. Q. Fenwick, J. M. Gregoire and O. R. Luca, *J. Photochem. Photobiol., B*, 2015, **152**, 47–57.
4 M. Ali, F. L. Zhou, K. Chen, C. Kotzur, C. L. Xiao, L. Bourgeois, X. Y. Zhang and D. R. MacFarlane, *Nat. Commun.*, 2016, **7**, 11335.
5 T. Oshikiri, K. Ueno and H. Misawa, *Angew. Chem., Int. Ed.*, 2016, **55**, 3942–3946.
6 Y. H. Cao, S. Z. Hu, F. Y. Li, Z. P. Fan, J. Bai, G. Lu and Q. Wang, *RSC Adv.*, 2016, **6**, 49862–49867.
7 C. J. M. van der Ham, M. T. M. Koper and D. G. H. Hetterscheid, *Chem. Soc. Rev.*, 2014, **43**, 5183–5191.
8 S. Giddey, S. P. S. Badwal and A. Kulkarni, *Int. J. Hydrogen Energy*, 2013, **38**, 14576–14594.
9 I. A. Amar, R. Lan, C. T. G. Petit and S. W. Tao, *J. Solid State Electrochem.*, 2011, **15**, 1845–1860.
10 V. Kordali, G. Kyriacou and C. Lambrou, *Chem. Commun.*, 2000, 1673–1674.
11 F. Kosaka, N. Noda, T. Nakamura and J. Otomo, *J. Mater. Sci.*, 2017, **52**, 2825–2835.
12 E. Vasileiou, V. Kyriakou, I. Garagounis, A. Vourros, A. Manerbino, W. G. Coors and M. Stoukides, *Solid State Ionics*, 2016, **288**, 357–362.
13 I. Garagounis, V. Kyriakou, A. Skodra, E. Vasileiou and M. Stoukides, *Energy Res.*, 2014, **2**.
14 V. Kyriakou, I. Garagounis, E. Vasileiou, A. Vourros and M. Stoukides, *Catal. Today*, 2017, **286**, 2–13.
15 J. N. Renner, L. F. Greenlee, K. E. Ayres and A. M. Herring, *Electrochem. Soc. Interface*, 2015, **24**, 51–57.
16 C. G. Yiokari, G. E. Pitselis, D. G. Polydoros, A. D. Katsaounis and C. G. Vayenas, *J. Phys. Chem. A*, 2000, **104**, 10600–10602.
17 Y. H. Xie, J. E. Wang, R. Q. Liu, X. T. Su, Z. P. Sun and Z. J. Li, *Solid State Ionics*, 2004, **168**, 117–121.
18 X. T. Su, R. Q. Liu and J. D. Wang, *Acta Chim. Sin. (Engl. Ed.)*, 2003, **61**, 505–509.
19 D. S. Yun, J. H. Joo, J. H. Yu, H. C. Yoon, J.-N. Kim and C.-Y. Yoo, *J. Power Sources*, 2015, **284**, 245–251.
20 R. Lan, K. A. Alkhazmi, I. A. Amar and S. Tao, *Appl. Catal., B*, 2014, **152**, 212–217.
21 I. A. Amar, R. Lan, C. T. G. Petit and S. Tao, *Electrocatalysis*, 2015, **6**, 286–294.
22 R. Lan, J. T. S. Irvine and S. Tao, *Sci. Rep.*, 2013, **3**, 1145.
23 K. Kim, N. Lee, C. Y. Yoo, J. N. Kim, H. C. Yoon and J. I. Han, *J. Electrochem. Soc.*, 2016, **163**, F610–F612.
24 F. Köleli and D. B. Kayan, *J. Electroanal. Chem.*, 2010, **638**, 119–122.
25 K. Kugler, M. Luhn, J. A. Schramm, K. Rahimi and M. Wessling, *Phys. Chem. Chem. Phys.*, 2015, **17**, 3768–3782.
26 S. Chen, S. Perathoner, C. Ampelli, C. Mebrahtu, D. Su and G. Centi, *Angew. Chem., Int. Ed.*, 2017, **56**, 2699–2703.
27 D. Bao, Q. Zhang, F.-L. Meng, H.-X. Zhong, M.-M. Shi, Y. Zhang, J.-M. Yan, Q. Jiang and X.-B. Zhang, *Adv. Mater.*, 2017, **29**, 1604799.
28 S. Licht, B. Cui, B. Wang, F.-F. Li, J. Lau and S. Liu, *Science*, 2014, **345**, 637–640.
29 D. Zhu, L. H. Zhang, R. E. Ruther and R. J. Hamers, *Nat. Mater.*, 2013, **12**, 836–841.
30 Y. Zhao, Yu. Zhao, G. I. N. Waterhouse, L. Zheng, X. Cao, F. Teng, L. Wu, C. Tung, D. O'Hare and T. Zhang, *Adv. Mater.*, 2017, **29**, 1703828.
31 A. Banerjee, B. D. Yuhas, E. A. Margulies, Y. B. Zhang, Y. Shim, M. R. Wasielewski and M. G. Kanatzidis, *J. Am. Chem. Soc.*, 2015, **137**, 2030–2034.
32 H. Li, J. Shang, Z. H. Ai and L. Z. Zhang, *J. Am. Chem. Soc.*, 2015, **137**, 6393–6399.

33 Y. Abghoui, A. L. Garden, V. F. Hlynsson, S. Bjorgvinsdottir, H. Olafsdottir and E. Skulason, *Phys. Chem. Chem. Phys.*, 2015, **17**, 4909–4918.
34 E. Skulason, T. Bligaard, S. Gudmundsdottir, F. Studt, J. Rossmeisl, F. Abild-Pedersen, T. Vegge, H. Jonsson and J. K. Norskov, *Phys. Chem. Chem. Phys.*, 2012, **14**, 1235–1245.
35 S. Back and Y. Jung, *Phys. Chem. Chem. Phys.*, 2016, **18**, 9161–9166.
36 N. Manh-Thuong, N. Seriani and R. Gebauer, *Phys. Chem. Chem. Phys.*, 2015, **17**, 14317–14322.
37 J. H. Montoya, C. Tsai, A. Vojvodic and J. K. Norskov, *ChemSusChem*, 2015, **8**, 2180–2186.
38 Y. Abghoui, A. L. Garden, J. G. Howat, T. Vegge and E. Skulason, *ACS Catal.*, 2016, **6**, 635–646.
39 L. M. Azofra, N. Li, D. R. MacFarlane and C. Sun, *Energy Environ. Sci.*, 2016, **9**, 2545–2549.
40 J. S. Anderson, J. Rittle and J. C. Peters, *Nature*, 2013, **501**, 84–87.
41 D. R. MacFarlane, M. Forsyth, P. C. Howlett, M. Kar, S. Passerini, J. M. Pringle, H. Ohno, M. Watanabe, F. Yan, W. J. Zheng, S. G. Zhang and J. Zhang, *Nat. Rev. Mater.*, 2016, **1**, 15.
42 D. R. MacFarlane, N. Tachikawa, M. Forsyth, J. M. Pringle, P. C. Howlett, G. D. Elliott, J. H. Davis, M. Watanabe, P. Simon and C. A. Angell, *Energy Environ. Sci.*, 2014, **7**, 232–250.
43 B. A. Rosen, A. Salehi-Khojin, M. R. Thorson, W. Zhu, D. T. Whipple, P. J. A. Kenis and R. I. Masel, *Science*, 2011, **334**, 643–644.
44 G. R. Zhang, M. Munoz and B. J. M. Etzold, *Angew. Chem., Int. Ed.*, 2016, **55**, 2257–2261.
45 S. Stevanovic and M. F. C. Gomes, *J. Chem. Thermodyn.*, 2013, **59**, 65–71.
46 D. L. Boucher, J. A. Davies, J. G. Edwards and A. Mennad, *J. Photochem. Photobiol., A*, 1995, **88**, 53–64.
47 J. L. Anderson, J. K. Dixon and J. F. Brennecke, *Accounts Chem. Res.*, 2007, **40**, 1208–1216.

